

The Color-Clinical Decoupling: Why Perceptual Calibration Fails Clinical Biomarkers in Smartphone Dermatology

Sungwoo Kang

Department of Electrical and Computer Engineering, Korea University, Seoul 02841, R
Email: krml919@korea.ac.kr

Abstract

Background: The rapid expansion of smartphone-based tele-dermatology assumes that colorimetric calibration—minimizing perceptual color error (ΔE)—ensures clinical reliability. This assumption remains untested at scale, particularly for underrepresented skin phototypes (Fitzpatrick III–IV).

Objective: To investigate whether standard colorimetric calibration translates to clinical biomarker reliability, and to identify the dominant sources of variance in cross-device skin color measurement.

Methods: We analyzed a total dataset of 43,424 images from 965 Korean subjects (Fitzpatrick III–IV) using the AI Hub Korean Skin Condition Measurement dataset. Cross-device comparisons utilized 14,475 matched front-facing images (4,825 per device) acquired across DSLR, tablet, and smartphone devices. Linear Color Correction Matrix (CCM) normalization—the industry standard—was applied to align consumer devices to a DSLR reference. Performance was assessed using CIEDE2000 color differences (ΔE) and Intraclass Correlation Coefficients (ICC) for Melanin Index, Erythema Index, and Individual Typology Angle (ITA).

Results: Raw smartphone images were clinically unusable: mean ΔE values of 8.26 (tablet) and 6.99 (smartphone) versus DSLR, with **0% of images** meeting the clinical acceptability threshold ($\Delta E < 2$). Linear CCM successfully reduced color error by 67–77%, achieving near-clinical color accuracy ($\Delta E < 2.3$). However, this colorimetric success **did not translate to clinical reliability**. Despite perceptually accurate colors, ITA showed poor inter-device agreement (ICC = 0.46), while Melanin Index achieved good agreement (ICC = 0.77). We term this divergence “color-clinical decoupling.” Critically, this decoupling disproportionately affects darker skin types: ITA sensitivity to b^* errors ranges from $\sim 1.7^\circ/\text{unit}$ for light skin (Type II/III) to $> 4.5^\circ/\text{unit}$ for dark skin (Type VI), representing a “metrological bias” against underrepresented populations. This decoupling is further compounded by anatomical factors: facial region accounts for 25.2% of color variance— $3.6\times$ greater than device effects (7.0%)—explaining why single-patch calibration protocols fail.

Conclusions: Standard colorimetric calibration creates false confidence: perceptually accurate images can yield unreliable clinical biomarkers. The ITA formula’s disproportionate sensitivity to b^* channel errors—the noisiest color component—explains

this decoupling mathematically. The dominance of anatomical variance over device variance challenges single-patch calibration assumptions and demands region-aware protocols. These findings establish that current smartphone dermatology standards are insufficient for clinical-grade biomarker extraction.

Keywords: tele-dermatology, color-clinical decoupling, smartphone validation, ITA, skin colorimetry, calibration failure, Fitzpatrick skin type

1 Introduction

The proliferation of smartphone-based dermatological applications has created unprecedented opportunities for remote skin health monitoring. [1, 2] Deep learning systems have demonstrated expert-level performance in melanoma classification, [3, 4] fueling expectations that consumer devices could enable accessible platforms for quantitative skin analysis. Central to this vision is an implicit assumption: that colorimetric calibration—the minimization of perceptual color error (ΔE)—ensures clinical reliability for derived biomarkers.

This assumption has never been rigorously tested.

The optical complexity of human skin presents fundamental challenges for camera-based colorimetry. Skin functions as a multilayered turbid medium, with color determined by the absorption spectra of melanin in the epidermis and hemoglobin in the dermal vasculature. [5, 6] When this continuous spectral information is sampled by RGB sensors, the fine spectral detail required to separate chromophore contributions is irreversibly lost. [7, 8] Device-specific variations compound this limitation: different sensors produce inconsistent RGB values for identical skin samples due to variations in spectral sensitivities and image signal processing (ISP) pipelines. [9, 10]

The standard solution—linear Color Correction Matrix (CCM) normalization—transforms

device RGB values toward a reference standard by minimizing the Euclidean distance in color space. [11, 12] This approach optimizes for perceptual color fidelity, as measured by the CIEDE2000 color difference formula (ΔE_{00}). [13, 14] The clinical acceptability threshold of $\Delta E < 2$ corresponds to the just-noticeable difference in human color perception. [15]

However, clinical skin color indices are not simple Euclidean distances. The Individual Typology Angle (ITA), widely used for Fitzpatrick skin type classification, [16, 17] is computed as an *arctangent ratio*:

$$\text{ITA} = \arctan\left(\frac{L^* - 50}{b^*}\right) \times \frac{180}{\pi} \quad (1)$$

This angular metric exhibits fundamentally different error sensitivity than the distance-based ΔE formula. A calibration that minimizes Euclidean color error may still harbor residual errors in specific color channels that are amplified by ratio-based clinical formulas.

Prior research has validated smartphone telemedicine for specific conditions, [18, 19] developed multi-device domain adaptation for other imaging modalities, [20–22] and established RGB-based chromophore quantification methods. [23, 24] However, these studies predominantly utilized datasets composed of Fitzpatrick I–II skin types, [25, 26] and none systematically tested whether colorimetric calibration guarantees clinical biomarker preservation.

This study addresses this critical gap. Using 43,424 images from 965 Korean subjects (Fitzpatrick III–IV), we test the hypothesis that standard colorimetric calibration ensures clinical reliability. Our investigation reveals three key findings:

1. **Color-Clinical Decoupling:** We introduce and systematically investigate “color-clinical decoupling”—the phenomenon where perceptually accurate calibration ($\Delta E <$

2.3) fails to preserve clinical biomarkers. While prior work has identified ITA measurement limitations including sensitivity to illuminants, [27] this is the first systematic demonstration that standard colorimetric calibration creates false clinical confidence, with ITA showing poor agreement ($ICC = 0.46$) despite excellent color fidelity. We provide mathematical derivation explaining this phenomenon through the differential sensitivity of ratio-based formulas to channel-specific errors.

2. **Calibration Protocol Failure:** We demonstrate that anatomical region variance (25.2%) exceeds device variance (7.0%) by $3.6\times$, providing empirical evidence that single-patch calibration—the current industry standard—cannot address the dominant source of measurement error.
3. **Fitzpatrick III–IV Benchmark:** We provide the first large-scale multi-device benchmark specifically for the “forgotten middle” of the skin tone spectrum, addressing a critical gap in algorithmic fairness.

These findings establish that current smartphone dermatology standards create false confidence: images that “look correct” may “diagnose incorrectly.” We argue that the field must move beyond perceptual color metrics toward biomarker-aware calibration paradigms.

2 Background and Related Work

2.1 Optical Properties of Human Skin

Human skin functions as a multilayered turbid medium whose appearance is governed by the interplay of absorption and scattering within the epidermis and dermis. [5, 28] The two

principal chromophores are melanin, concentrated in the basal layer of the epidermis, and hemoglobin, distributed within the dermal vasculature. [6] Melanin exhibits broadband absorption across the visible spectrum, decreasing monotonically from 300 to 700 nm. Oxyhemoglobin displays characteristic absorption peaks at 542 nm and 577 nm, and blood stasis patterns further modulate perceived skin pigmentation. [7, 29]

The spectral reflectance of skin results from a complex light transport process involving specular reflection at the stratum corneum, volumetric scattering within the dermis, and wavelength-dependent absorption at varying depths. [30, 31] RGB sensors integrate this continuous spectrum into three broad channels, irreversibly discarding the fine spectral detail required to deconvolve individual chromophore contributions—a limitation arising from metamerism.

2.2 Device-Dependent Color Rendering

Modern digital cameras exhibit substantial variability in color reproduction due to differences in sensor design and ISP pipelines. [10] Three primary sources of device dependence exist: (1) spectral sensitivity functions of color filter arrays vary across manufacturers; [11, 32] (2) ISP pipelines apply nonlinear transformations including gamma correction, tone mapping, and “memory color” optimization; [10, 12] and (3) the sRGB color space provides limited gamut and introduces quantization errors in dark tones.

These limitations motivate the use of Color Correction Matrices (CCMs) to transform camera RGB values toward device-independent references. [11] While linear CCMs provide computational efficiency, polynomial extensions have demonstrated improved accuracy for

strongly nonlinear responses. [9, 12]

2.3 Clinical Skin Color Indices

Quantitative dermatology employs several derived indices to characterize skin pigmentation. The Individual Typology Angle (ITA) provides an objective correlate of Fitzpatrick skin phototype. [16, 17, 33] The Melanin Index, computed from L^* using logarithmic transformations, correlates with epidermal melanin concentration. [16, 24] The Erythema Index, derived from the a^* channel, reflects dermal hemoglobin content. [34, 35] Critically, while device validation studies have assessed inter-device agreement for individual indices, no prior work has systematically compared how different clinical metrics—with their distinct mathematical structures—respond to identical calibration procedures. This gap is significant: a calibration optimized for one index may fail another.

2.4 The Implicit Assumption of Colorimetric Calibration

The field of tele-dermatology operates under an unstated assumption: minimizing perceptual color error (ΔE) guarantees clinical validity. This assumption conflates two distinct objectives—visual fidelity and diagnostic accuracy—that may require fundamentally different optimization targets.

The CIEDE2000 formula was designed to correlate with human perceptual discrimination: [13, 14]

$$\Delta E_{00} = \sqrt{\left(\frac{\Delta L'}{k_L S_L}\right)^2 + \left(\frac{\Delta C'}{k_C S_C}\right)^2 + \left(\frac{\Delta H'}{k_H S_H}\right)^2 + R_T \frac{\Delta C'}{k_C S_C} \frac{\Delta H'}{k_H S_H}} \quad (2)$$

This formula applies weighting functions that suppress errors humans perceive poorly while

emphasizing perceptually salient differences. Crucially, this perceptual optimization is *mis-aligned* with clinical needs.

Consider the ITA formula: $\arctan[(L^* - 50)/b^*]$. This is an *angular* metric in the L^* - b^* plane, fundamentally different from the *distance* metric of ΔE . Error propagation analysis reveals:

$$\delta(\text{ITA}) = \frac{\partial \text{ITA}}{\partial L^*} \delta L^* + \frac{\partial \text{ITA}}{\partial b^*} \delta b^* \quad (3)$$

where the partial derivatives are:

$$\frac{\partial \text{ITA}}{\partial L^*} = \frac{b^*}{(L^* - 50)^2 + (b^*)^2} \quad (4)$$

$$\frac{\partial \text{ITA}}{\partial b^*} = \frac{-(L^* - 50)}{(L^* - 50)^2 + (b^*)^2} \quad (5)$$

For typical skin colors in our dataset ($L^* \approx 75$, $b^* \approx 15$), equation (5) yields $|\partial \text{ITA} / \partial b^*| \approx 0.03 \text{ rad/unit} \approx 1.7^\circ/\text{unit}$. A seemingly small 1-unit error in b^* produces a 1.7° shift in ITA—sufficient to cross Fitzpatrick skin type boundaries—while contributing only ~ 1 to the ΔE calculation. Notably, perceptibility thresholds differ across CIELAB axes, with the b^* (blue-yellow) axis generally exhibiting higher tolerance thresholds than L^* or a^* , meaning b^* errors are both less perceptible and more clinically consequential.

The b^* channel is derived primarily from the blue sensor. Due to the shallow absorption depth of blue photons in silicon and the spectral deficiency of common indoor illuminants, the effective signal-to-noise ratio of the blue channel is significantly lower than that of the green channel. [36, 37] Shot noise scales as $\sigma \propto 1/\sqrt{QE}$, making blue the noisiest channel.

This noise propagates through sRGB-to-CIELAB transformation and is *amplified* by the ITA formula’s sensitivity to b^* .

Linear CCM minimizes the L_2 norm of color error:

$$\min_{\mathbf{A}, \mathbf{b}} \sum_{i=1}^N \left\| \mathbf{A} \cdot \text{RGB}_i + \mathbf{b} - \text{RGB}_{\text{ref}}^{(i)} \right\|_2^2 \quad (6)$$

This optimization reduces errors *uniformly* across color channels, but ITA requires *disproportionate* reduction in b^* errors. The result: a calibration can achieve $\Delta E < 2$ while harboring b^* residuals that produce clinically significant ITA discrepancies.

We term this phenomenon **color-clinical decoupling**: the divergence between perceptual color accuracy and clinical biomarker reliability.

2.5 Dataset Bias in Dermatological AI

Dermatological AI systems suffer from severe demographic imbalances. [25, 38] The ISIC Archive and other benchmarks are predominantly composed of Fitzpatrick I–II types, with limited representation of darker skin. [26, 39] Furthermore, the Fitzpatrick scale itself conflates race with photosensitivity, limiting its utility for diverse populations. [40] Critically, intermediate skin tones (Fitzpatrick III–IV)—common in East Asian, Hispanic, and Mediterranean populations—represent a “forgotten middle” that is neither the focus of fairness initiatives targeting darker skin nor well-represented in existing light-skin-dominated datasets.

While underrepresentation of darker skin types in dermatological AI is well-documented, [26, 38, 39] our dataset of 43,424 images from 965 Korean subjects (Fitzpatrick III–IV) represents the largest cohort specifically designed to evaluate color-clinical decoupling in this un-

derrepresented population, providing systematic characterization of device-dependent color rendering.

3 Materials and Methods

3.1 Dataset

This study utilized the Korean Skin Condition Measurement dataset from AI Hub (ai-hub.or.kr), a publicly available resource for dermatological research. [41] The dataset comprises standardized facial images captured under controlled lighting conditions.

3.1.1 Subject Demographics

A total of 965 subjects were included:

- **Age groups:** ≤ 30 years (n=2,950 samples), 31–45 years (n=2,590), 46–60 years (n=2,570), > 60 years (n=1,540)
- **Gender:** Female (n=4,830 samples), Male (n=4,820 samples)
- **Fitzpatrick skin types:** Predominantly Types III–IV

3.1.2 Imaging Devices

Three device categories were employed:

1. **DSLR (Reference):** Professional-grade camera under controlled dark room lighting, capturing 7 viewing angles (front, front-top, front-bottom, left 15°, left 30°, right 15°, right 30°)

2. **Tablet:** Consumer-grade tablet camera, capturing 3 viewing angles (front, left, right)
3. **Smartphone:** Consumer-grade smartphone camera, capturing 3 viewing angles (front, left, right)

The analyzed dataset comprises 43,424 samples: DSLR (33,774 samples across 7 angles), tablet (4,825 front-facing samples), and smartphone (4,825 front-facing samples). One DSLR sample was excluded due to invalid bounding box coordinates that prevented reliable color extraction. Although the source dataset includes 3 angles for consumer devices (totaling 14,475 samples per device), only the front-facing imagery was included in this study to maintain focus on cross-device consistency. For cross-device agreement analysis, these 14,475 matched front-facing samples (4,825 per device) ensured geometric alignment across all three platforms.

3.1.3 Facial Regions

Five standardized facial regions were analyzed: forehead, left cheek, right cheek, chin, and glabella.

3.2 Color Space Transformation

RGB values were transformed to CIELAB using D65 illuminant:

$$\text{RGB} \xrightarrow{\text{Gamma}} \text{Linear RGB} \xrightarrow{\text{D65}} \text{XYZ} \xrightarrow{\text{CIE}} L^*a^*b^* \quad (7)$$

3.3 Color Correction Matrix

Linear CCM normalization was performed using ordinary least squares:

$$\begin{bmatrix} R_{\text{corr}} \\ G_{\text{corr}} \\ B_{\text{corr}} \end{bmatrix} = \mathbf{A} \begin{bmatrix} R_{\text{src}} \\ G_{\text{src}} \\ B_{\text{src}} \end{bmatrix} + \mathbf{b} \quad (8)$$

where $\mathbf{A} \in \mathbb{R}^{3 \times 3}$ and $\mathbf{b} \in \mathbb{R}^3$. Validation employed 5-fold cross-validation with 80/20 train-test split.

3.4 Clinical Index Calculations

3.4.1 Melanin Index

$$\text{MI} = 100 \times \log_{10} \left(\frac{100}{L^*} \right) \quad (9)$$

3.4.2 Erythema Index

$$\text{EI} = a^* - 0.5 \times L^* \quad (10)$$

3.4.3 Individual Typology Angle

$$\text{ITA} = \arctan \left(\frac{L^* - 50}{b^*} \right) \times \frac{180}{\pi} \quad (11)$$

3.5 Statistical Analysis

Inter-device agreement was assessed using ICC(3,1) for absolute agreement. [42, 43] ICC interpretation: <0.50 (poor), 0.50–0.75 (moderate), 0.75–0.90 (good), >0.90 (excellent). [44]

Bland-Altman analysis characterized device agreement with 95% limits of agreement. [45]

ANOVA assessed factor influences on ΔE , with effect sizes quantified using eta-squared (η^2): 0.01 (small), 0.06 (medium), 0.14 (large). [46]

All analyses used Python 3.8 with scipy, pingouin, and statsmodels. Significance: $\alpha = 0.05$ with Bonferroni correction.

4 Results

4.1 Raw Device Performance: Clinical Unusability of Uncalibrated Images

Table 1 summarizes device characteristics. Consumer devices exhibited systematic underexposure relative to DSLR ($L^* = 72.7$ – 77.6 vs. 81.3) and compressed b^* values (8.96 – 10.12 vs. 17.59), as visualized in Figure 1 and Figure 2.

Table 1: Device characterization summary.

Parameter	DSLR	Tablet	Smartphone
N samples	33,774	4,825	4,825
Mean L^*	81.35	72.73	77.56
Mean a^*	7.95	6.08	5.68
Mean b^*	17.59	10.12	8.96
SNR (LAB)	37.5 dB	–	–

Table 2 presents inter-device color differences. Mean ΔE values of 8.26 (tablet) and 6.99 (smartphone) versus DSLR exceeded the clinical threshold ($\Delta E < 2$) by factors of 3–4 \times (Figure 3 and Figure 4). **Zero percent of raw images achieved clinical acceptability.**

Table 2: Inter-device CIEDE2000 color differences.

Device Pair	Mean	Std	Median	95th %ile
DSLR vs Tablet	8.26	2.70	7.57	13.71
DSLR vs Smartphone	6.99	1.84	6.77	10.37
Tablet vs Smartphone	4.47	2.39	4.13	8.97

This finding empirically demonstrates that raw smartphone images are clinically unusable for quantitative skin analysis without active calibration.

4.2 CCM Normalization: Colorimetric Success

Linear CCM substantially reduced color differences (Table 3 and Figure 5): 77.4% improvement for tablet (ΔE : 8.33 \rightarrow 1.88) and 67.4% for smartphone (7.02 \rightarrow 2.29). Post-normalization median values approached clinical acceptability (1.66 and 2.09 respectively).

Table 3: CCM normalization performance (5-fold cross-validation).

Transformation	ΔE Before	ΔE After	Improvement
Tablet \rightarrow DSLR	8.33 \pm 2.76	1.88 \pm 1.14	77.4%
Smartphone \rightarrow DSLR	7.02 \pm 1.78	2.29 \pm 1.22	67.4%

4.3 The Decoupling: Clinical Index Failure Despite Colorimetric Success

Despite effective colorimetric normalization, clinical index agreement varied dramatically (Table 4, Figure 6, and Figure 7). While Melanin Index achieved good agreement (ICC = 0.767), **ITA showed poor agreement (ICC = 0.455)**. This represents the central

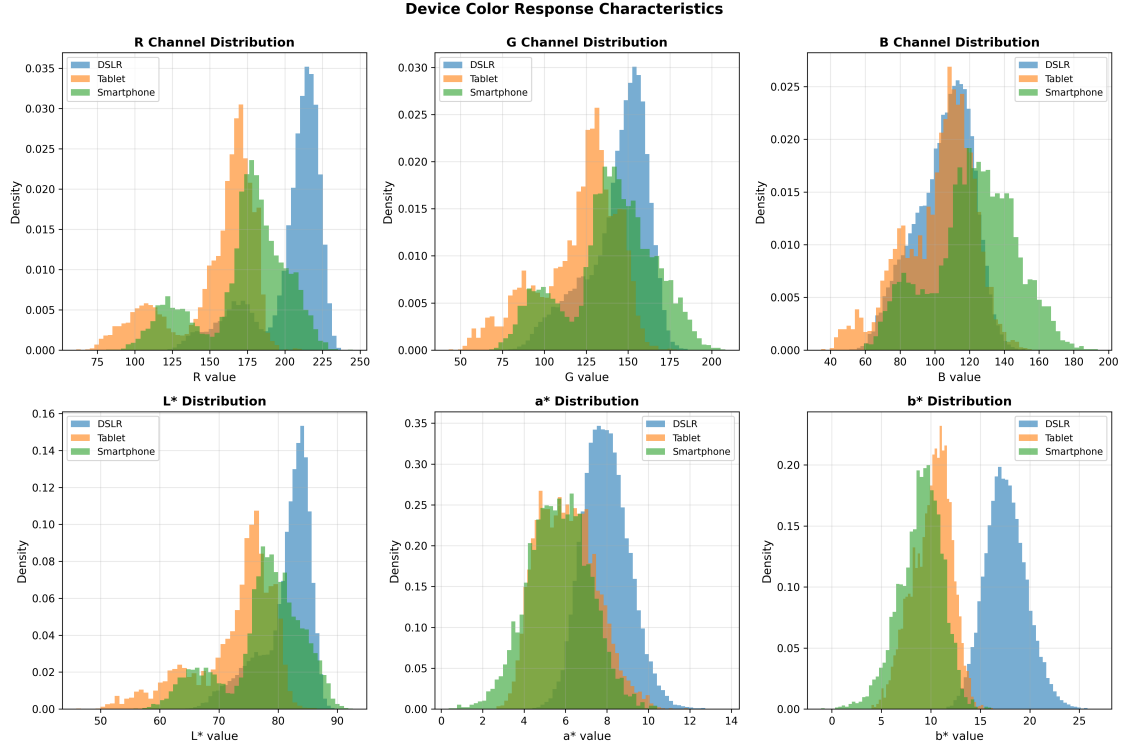


Figure 1: RGB and CIELAB color distributions across three imaging devices (DSLR, tablet, smartphone) for Korean skin samples (total $n=43,424$; cross-device comparison subset $n=14,475$). (A) RGB channel distributions showing device-specific color rendering characteristics. (B) CIELAB $L^*a^*b^*$ distributions demonstrating lightness and chromaticity variations across devices.

finding: perceptual color accuracy does not guarantee clinical biomarker reliability.

The pattern in Table 4 reveals the mechanism: b^* channel agreement ($ICC = 0.425$) is substantially lower than L^* ($ICC = 0.774$). Since ITA depends critically on b^* through its ratio formula, the poor b^* agreement propagates directly to ITA. In contrast, Melanin Index depends only on L^* and thus inherits the good L^* agreement.

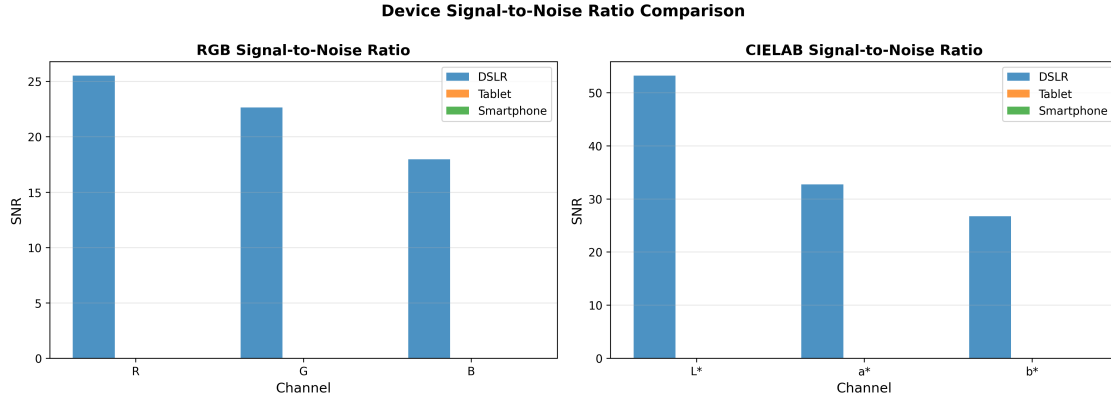


Figure 2: Signal-to-noise ratio (SNR) comparison across devices calculated from repeated measurements at multiple capture angles. Higher SNR values indicate better measurement precision and lower random noise. Error bars represent standard deviation across facial regions (forehead, left cheek, right cheek, chin, glabella).

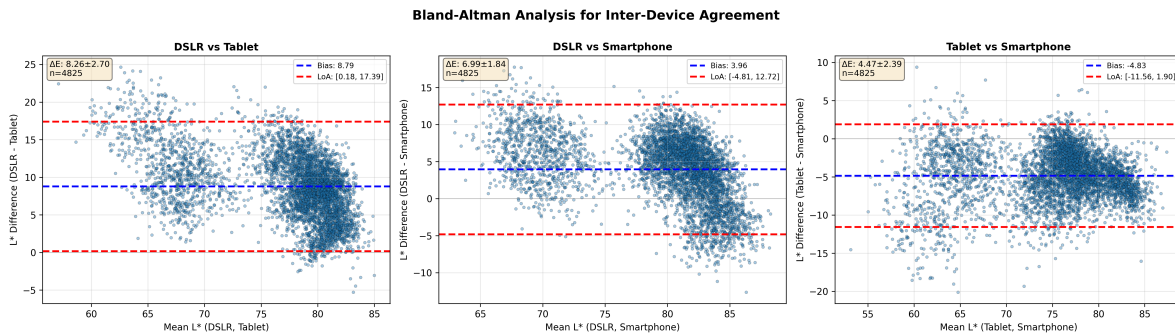


Figure 3: Bland-Altman plots comparing L^* , a^* , and b^* measurements between consumer devices (tablet, smartphone) and reference DSLR. Solid horizontal lines indicate mean bias; dashed lines show 95% limits of agreement (± 1.96 SD).

4.4 Sources of Variance: Implications for Calibration Protocol Design

ANOVA revealed a striking hierarchy of variance sources (Table 5 and Figure 8). **Facial anatomical region** accounted for **25.2%** of variance ($\eta^2 = 0.252$)—**3.6 times greater** than device hardware effects ($\eta^2 = 0.070$).

The chin region exhibited the largest color differences (mean $\Delta E = 9.63$), while the

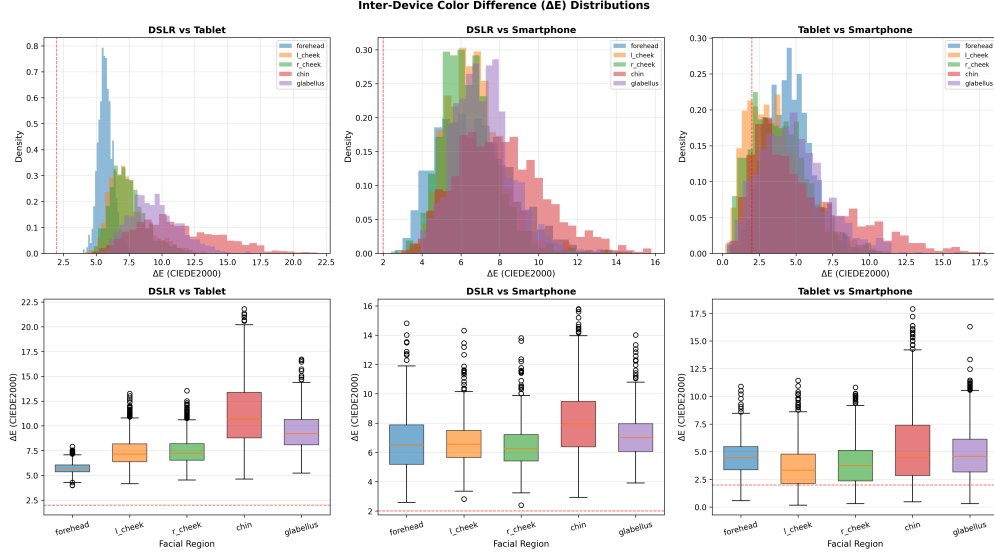


Figure 4: CIEDE2000 color difference (ΔE) distributions by facial region and source device. The vertical dashed line indicates the clinically perceptible threshold ($\Delta E = 2.0$). The chin region exhibits the largest color differences, while cheek regions show better inter-device agreement.

forehead showed better agreement (mean $\Delta E = 6.21$). This finding challenges the prevailing single-patch calibration paradigm: a correction matrix derived from cheek measurements may fail when applied to the forehead or chin.

5 Discussion

5.1 The Color-Clinical Decoupling Phenomenon

The central finding of this study is the **non-linear decoupling between colorimetric accuracy and clinical biomarker reliability**. Despite achieving near-clinical color fidelity ($\Delta E < 2.3$), the ITA index exhibited poor inter-device agreement ($ICC = 0.46$). This finding challenges the fundamental assumption underlying smartphone dermatology: that “looking correct” guarantees “diagnosing correctly.”

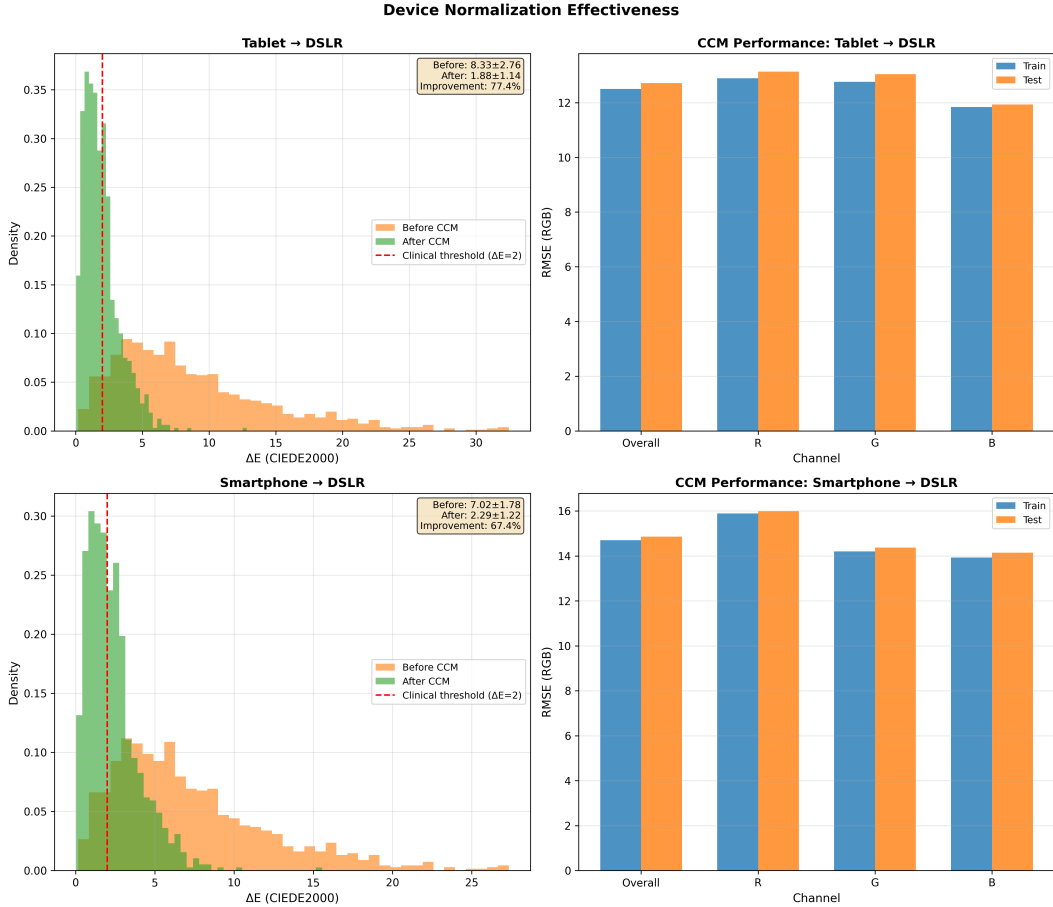


Figure 5: Color correction matrix (CCM) normalization results showing ΔE distributions before and after calibration. Post-normalization ΔE distributions demonstrate significant improvement, with linear CCM trained using 5-fold cross-validation.

The mathematical origins of this decoupling merit analysis. The CIEDE2000 formula measures a weighted Euclidean distance in color space, optimized for human perceptual discrimination. Linear CCM minimizes the L_2 norm of RGB residuals, distributing error reduction uniformly across channels. However, the ITA formula is not a distance—it is an arctangent ratio that exhibits singular behavior as b^* approaches zero and nonlinear amplification of b^* errors.

Table 4: Intraclass Correlation Coefficients for clinical indices and CIELAB channels.

Index/Channel	ICC(3,1)	95% CI	Interpretation
Melanin Index	0.767	[0.76, 0.78]	Good
Erythema Index	0.652	[0.64, 0.66]	Moderate
ITA	0.455	[0.44, 0.47]	Poor
L^*	0.774	[0.76, 0.78]	Good
a^*	0.550	[0.53, 0.57]	Moderate
b^*	0.425	[0.41, 0.44]	Poor

Table 5: ANOVA: Factors influencing inter-device ΔE (pre-normalization).

Factor	F-statistic	p-value	η^2	Effect Size
Facial Region	813.89	<0.001	0.252	Large
Source Device	728.56	<0.001	0.070	Medium
Gender	72.84	<0.001	0.007	Small
Skin Type	2.77	0.017	0.001	Small
Age Group	4.47	0.004	0.001	Small

From equations (4) and (5), for our dataset’s typical skin values ($L^* \approx 75$, $b^* \approx 15$):

$$\left| \frac{\partial \text{ITA}}{\partial b^*} \right| = \frac{|75 - 50|}{(75 - 50)^2 + 15^2} = \frac{25}{850} \approx 0.029 \text{ rad/unit} \approx 1.7^\circ/\text{unit} \quad (12)$$

A 1-unit residual in b^* —easily masked within a $\Delta E < 2$ calibration—produces a 1.7° shift in ITA. Since Fitzpatrick skin type boundaries span approximately 10° in ITA, [17] a 3-unit b^* error can cause skin type misclassification.

Critically, this sensitivity is phenotype-dependent. The ITA sensitivity formula $|\partial \text{ITA} / \partial b^*| = |L^* - 50| / [(L^* - 50)^2 + (b^*)^2]$ reveals that darker skin types—characterized by lower L^* values closer to 50 and lower b^* values—experience dramatically amplified error sensitivity. For Type V skin ($L^* \approx 60$, $b^* \approx 10$), the sensitivity increases to $\sim 2.9^\circ/\text{unit}$; for

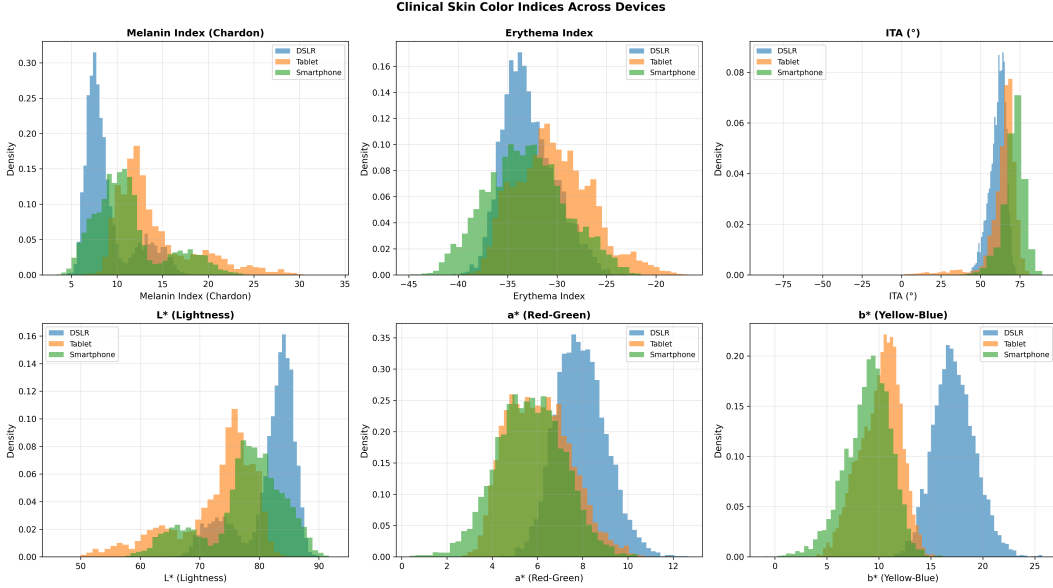


Figure 6: Comparison of clinical skin color indices across devices after CCM normalization. (A) Melanin Index distributions. (B) Erythema Index distributions. (C) Individual Typology Angle (ITA) for Fitzpatrick skin type classification.

Type VI skin ($L^* \approx 40$, $b^* \approx 5$), it reaches $\sim 4.6^\circ/\text{unit}$. A 2-unit calibration residual in b^* —perceptually negligible—produces a 3.4° shift in ITA for light skin but a **9.2° shift for dark skin**. This represents a “metrological bias”: current calibration protocols, by optimizing for average ΔE , do not suppress b^* errors with the aggression required for accurate assessment of darker skin tones. Table 6 summarizes this phenotype-dependent vulnerability.

The blue sensor’s inherently low quantum efficiency produces elevated shot noise that propagates directly to b^* . Linear CCM, optimized for overall color fidelity, cannot selectively suppress this critical error source. The result is “color-clinical decoupling”: colorimetric success masking clinical failure.

In contrast, the Melanin Index formula $MI = 100 \times \log_{10}(100/L^*)$ depends solely on L^* , which benefits from higher signal-to-noise in the green channel. This explains why Melanin Index achieved good agreement ($ICC = 0.77$) while ITA failed—the two indices sample

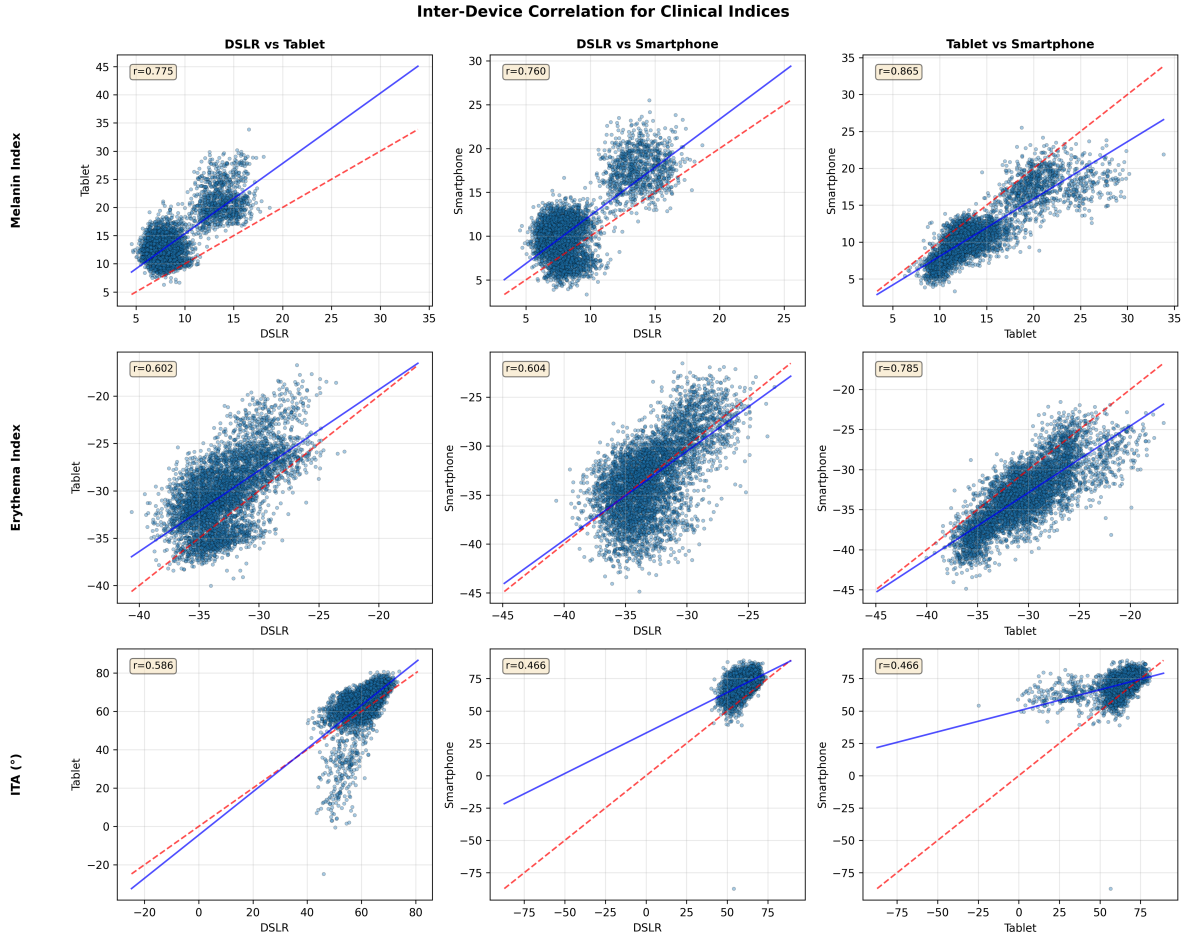


Figure 7: Pearson correlation plots comparing clinical indices between consumer devices and DSLR reference. Each point represents a matched sample (same subject, same facial region). Diagonal dashed line indicates perfect agreement ($r = 1.0$).

different axes of the colorimetric error ellipsoid, with ITA maximally sensitive to the noisiest component.

This finding has immediate implications for tele-dermatology: standard colorimetric calibration, the current industry norm, is **insufficient** for clinical applications requiring ITA or similar ratio-based biomarkers.

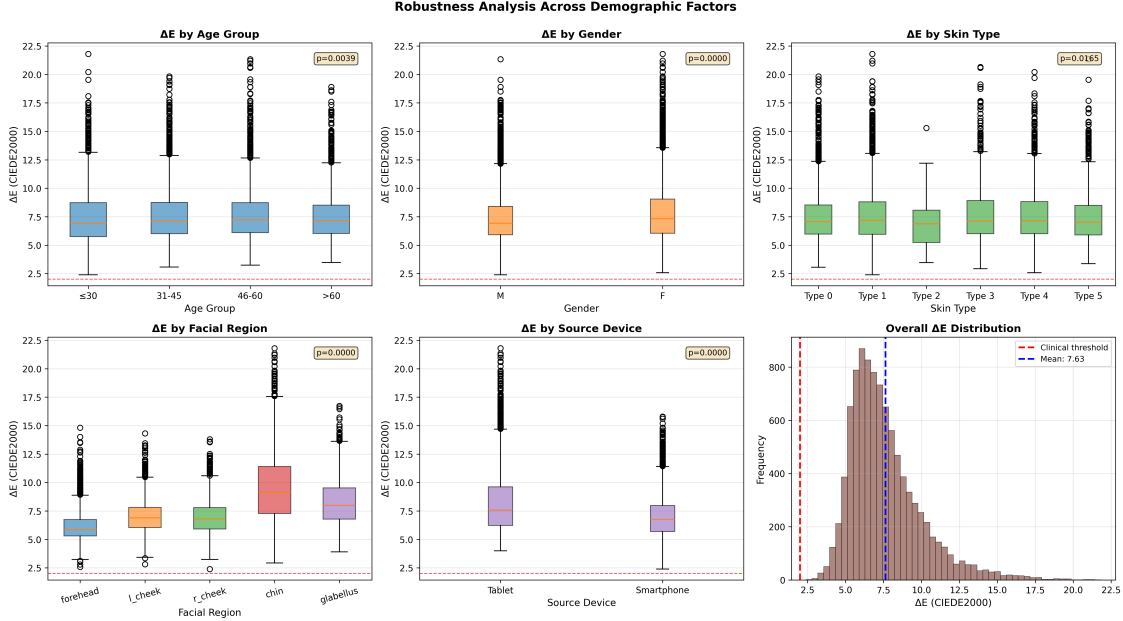


Figure 8: Stratified analysis of pre-normalization color differences (ΔE) across demographic factors. (A) Age groups. (B) Gender. (C) Fitzpatrick skin type. (D) Facial region. One-way ANOVA revealed significant effects for all factors, with facial region showing the largest effect size.

5.2 Why Single-Patch Calibration Fails

The color-clinical decoupling is further exacerbated by an overlooked calibration assumption: that facial skin is a uniform surface. While regional variation in facial skin color is well-documented—studies have shown significant differences in color indices between forehead, cheek, and chin regions [47, 48]—prior work has not quantified regional variance as a proportion of total variance nor compared it against device variance. Our ANOVA analysis reveals this assumption to be fundamentally flawed: facial region explains 25.2% of color variance, exceeding device effects (7.0%) by a factor of 3.6—the first such quantitative decomposition.

This “anatomical dominance” arises from multiple physiological sources. The T-zone (forehead and glabella) exhibits higher sebaceous gland density than cheek regions, resulting

Table 6: Phenotype-dependent ITA sensitivity to b^* channel errors. Sensitivity calculated from $|\partial\text{ITA}/\partial b^*| = |L^* - 50|/[(L^* - 50)^2 + (b^*)^2]$. The “2-unit Error Impact” shows the ITA shift from a typical calibration residual, demonstrating disproportionate effects on darker skin types.

Skin Type	L^*	b^*	Sensitivity ($^\circ$/unit)	2-unit Error Impact
Type II/III (Light)	75	15	1.68	3.4 $^\circ$
Type IV (Intermediate)	65	15	1.92	3.8 $^\circ$
Type V (Brown)	60	10	2.86	5.7 $^\circ$
Type VI (Dark)	40	5	4.58	9.2$^\circ$

in elevated sebum secretion that alters surface optical properties. [49] Sebum functions as an index-matching fluid ($n \approx 1.46$), reducing the refractive index mismatch at the stratum corneum ($n \approx 1.55$) via the optical clearing effect. [28, 50] This reduction in refractive index discontinuity decreases surface scattering, allowing more photons to penetrate deeper into the epidermis and dermis where they interact with melanin and hemoglobin—producing “richer” or “darker” apparent skin color (lower L^* , higher chroma). Simultaneously, the smooth liquid sebum surface produces intense specular highlights under directional illumination. [31] These regional optical variations produce angle-dependent color shifts that a single CCM cannot correct.

Facial skin thickness varies substantially: the periorbital region is among the thinnest (0.5–1.0 mm), while chin and forehead are thicker (1.5–2.0 mm). [51] Since skin color arises from chromophore absorption at specific depths, thickness variations alter the optical path length and relative contributions of melanin versus hemoglobin.

The chin region, exhibiting the largest color differences (mean $\Delta E = 9.63$), presents a particularly challenging case due to pronounced surface curvature creating geometric variations in illumination.

This finding invalidates single-patch calibration protocols: a CCM derived from cheek measurements may fail when applied to forehead or chin. Future calibration must be **region-aware**, with region-specific corrections or spatially-varying calibration fields based on facial landmark detection.

5.3 Implications for Tele-Dermatology Standards

Our findings have critical implications for smartphone dermatology. First, the 0% raw acceptability rate proves that uncalibrated consumer devices are clinically unusable for quantitative analysis. The widespread practice of using raw smartphone images for AI training likely introduces device-specific biases that obscure pathological signals. [25, 38]

Second, even with calibration, the color-clinical decoupling renders current standards inadequate for ITA-dependent applications, including Fitzpatrick skin type classification and melanoma risk assessment. Clinical applications must either: (a) avoid ratio-based indices, (b) develop biomarker-aware calibration that explicitly minimizes ITA error, or (c) employ uncertainty quantification to flag unreliable measurements.

Third, interestingly, gender also showed a statistically significant difference ($p < 0.001$). Although its influence ($\eta^2 = 0.007$) is small compared to facial region, this suggests that camera ISPs may exhibit differential behavior across demographics. If “universal” CCMs are derived from specific populations, they may embed demographic biases—a fairness concern for global health applications. [26, 39]

5.4 Limitations

Several limitations should be acknowledged. First, we identified the decoupling phenomenon but did not implement non-linear or biomarker-aware corrections; such approaches remain for future investigation. Second, our dataset was restricted to healthy skin; pathological tissue may exhibit different spectral properties. Third, the population was limited to Korean subjects (Fitzpatrick III–IV); generalization to types I–II and V–VI requires additional study. Fourth, controlled lighting conditions may not represent real-world acquisition environments.

5.5 Future Directions

The color-clinical decoupling motivates several research directions:

Biomarker-Specific Loss Functions. Composite losses combining perceptual ($\mathcal{L}_{\Delta E}$) and clinical (\mathcal{L}_{ITA}) terms could optimize simultaneously for visual fidelity and diagnostic accuracy, explicitly penalizing b^* errors.

Region-Aware Calibration. Modern facial landmark detection enables region-specific CCMs or spatially-varying correction fields accounting for local optical properties.

Spectral Reconstruction. Methods recovering hyperspectral reflectance from RGB inputs [52, 53] could compute clinical indices from chromophore spectra rather than device-dependent colors, potentially resolving the decoupling.

Physics-Informed Neural Networks. PINNs embedding radiative transfer constraints [54] could enforce biophysically plausible chromophore concentrations.

Multi-Ethnic Benchmark Extension. Extension to Fitzpatrick I–VI and the Monk Skin Tone scale [55] is essential for equitable algorithm development.

6 Conclusion

This study establishes that standard colorimetric calibration in smartphone dermatology creates false confidence: perceptually accurate images can yield unreliable clinical biomarkers. Using 43,424 images from 965 Korean subjects across DSLR, tablet, and smartphone devices, we demonstrate a fundamental “color-clinical decoupling” phenomenon.

Our key findings are:

1. **Raw images are clinically unusable:** 0% of uncalibrated consumer device images met the $\Delta E < 2$ clinical threshold, with mean errors of 6.99–8.26.
2. **Standard calibration fails clinical needs:** Linear CCM achieved 67–77% color error reduction ($\Delta E < 2.3$), yet ITA showed poor inter-device agreement ($\text{ICC} = 0.46$) versus good Melanin Index agreement ($\text{ICC} = 0.77$). This failure is compounded by anatomical factors: facial region accounts for 25.2% of color variance— $3.6\times$ greater than device effects—meaning single-patch calibration cannot address the dominant error source.
3. **Calibration errors disproportionately affect darker skin:** ITA sensitivity to b^* errors increases from $\sim 1.7^\circ/\text{unit}$ for light skin (Type II/III) to $> 4.5^\circ/\text{unit}$ for dark skin (Type VI). A 2-unit calibration residual produces a 3.4° ITA shift in light skin but a 9.2° shift in dark skin—sufficient to cause skin type misclassification. This “metrological bias” means current calibration protocols fail to protect the most vulnerable populations from measurement error.

Additionally, this work provides the first large-scale multi-device benchmark specifically

for Fitzpatrick III–IV skin tones, addressing the “forgotten middle” in algorithmic fairness research.

The color-clinical decoupling arises from a mathematical mismatch: ΔE is a distance metric while ITA is an angular ratio disproportionately sensitive to b^* errors—the noisiest color channel. Linear CCM, minimizing overall color distance, cannot selectively suppress this critical error source.

These findings argue that tele-dermatology must move beyond perceptual color metrics toward biomarker-aware calibration paradigms. Current smartphone apps using ITA for skin type classification may be producing unreliable results even when images “look correct.” Future calibration protocols must be region-aware, biomarker-specific, and validated on diverse populations to ensure both accuracy and algorithmic fairness.

Disclosures

The authors declare no conflicts of interest.

Code, Data, and Materials Availability

The Korean Skin Condition Measurement dataset is available through AI Hub (aihub.or.kr) under restricted research access. Analysis code will be available on GitHub upon publication.

References

- [1] Andre Esteva, Brett Kuprel, Roberto A Novoa, Justin Ko, Susan M Swetter, Helen M Blau, and Sebastian Thrun. Dermatologist-level classification of skin cancer with deep neural networks. *nature*, 542(7639):115–118, 2017.

- [2] Holger A Haenssle, Christine Fink, Roland Schneiderbauer, Ferdinand Toberer, Timo Buhl, Andreas Blum, Aadi Kaloo, A Ben Hadj Hassen, Luc Thomas, Alexander Enk, et al. Man against machine: diagnostic performance of a deep learning convolutional neural network for dermoscopic melanoma recognition in comparison to 58 dermatologists. *Annals of oncology*, 29(8):1836–1842, 2018.
- [3] Michael A Marchetti, Noel CF Codella, Stephen W Dusza, David A Gutman, Brian Helba, Aadi Kaloo, Nabin Mishra, Cristina Carrera, M Emre Celebi, Jennifer L DeFazio, et al. Results of the 2016 international skin imaging collaboration international symposium on biomedical imaging challenge: Comparison of the accuracy of computer algorithms to dermatologists for the diagnosis of melanoma from dermoscopic images. *Journal of the American Academy of Dermatology*, 78(2):270–277, 2018.
- [4] Titus J Brinker, Achim Hekler, Alexander H Enk, Joachim Klode, Axel Hauschild, Carola Berking, Bastian Schilling, Sebastian Haferkamp, Dirk Schadendorf, Tim Holland-Letz, et al. Deep learning outperformed 136 of 157 dermatologists in a head-to-head dermoscopic melanoma image classification task. *European Journal of Cancer*, 113:47–54, 2019.
- [5] Steven L Jacques. Optical properties of biological tissues: a review. *Physics in Medicine & Biology*, 58(11):R37, 2013.
- [6] R Rox Anderson and John A Parrish. The optics of human skin. *Journal of investigative dermatology*, 77(1):13–19, 1981.
- [7] George Zonios, Julie Bykowski, and Nikiforos Kollias. Skin melanin, hemoglobin, and light scattering properties can be quantitatively assessed in vivo using diffuse reflectance spectroscopy. *Journal of Investigative Dermatology*, 117(6):1452–1457, 2001.
- [8] Izumi Nishidate, Yoshihisa Aizu, and Hiromichi Mishina. Estimation of melanin and hemoglobin in skin tissue using multiple regression analysis aided by monte carlo simulation. *Journal of biomedical optics*, 9(4):700–710, 2004.
- [9] Graham D Finlayson, Michal Mackiewicz, and Anya Hurlbert. Color correction using root-polynomial regression. *IEEE Transactions on Image Processing*, 24(5):1460–1470, 2015.
- [10] Hakki Can Karaimer and Michael S Brown. A software platform for manipulating the camera imaging pipeline. In *European Conference on Computer Vision*, pages 429–444. Springer, 2016.
- [11] Guowei Hong, M Ronnier Luo, and Peter A Rhodes. A study of digital camera colorimetric characterization based on polynomial modeling. *Color research & application: Endorsed by inter-society color council, The colour group (Great Britain), Canadian society for color, color science association of Japan, Dutch society for the study of color, The Swedish colour centre foundation, colour society of Australia, Centre Français de la Couleur*, 26(1):76–84, 2001.

- [12] Vien Cheung, Stephen Westland, David Connah, and Caterina Ripamonti. A comparative study of the characterisation of colour cameras by means of neural networks and polynomial transforms. *Coloration technology*, 120(1):19–25, 2004.
- [13] Gaurav Sharma, Wencheng Wu, and Edul N Dalal. The ciede2000 color-difference formula: Implementation notes, supplementary test data, and mathematical observations. *Color Research & Application: Endorsed by Inter-Society Color Council, The Colour Group (Great Britain), Canadian Society for Color, Color Science Association of Japan, Dutch Society for the Study of Color, The Swedish Colour Centre Foundation, Colour Society of Australia, Centre Français de la Couleur*, 30(1):21–30, 2005.
- [14] M Ronnier Luo, Guihua Cui, and Bryan Rigg. The development of the cie 2000 colour-difference formula: Ciede2000. *Color Research & Application: Endorsed by Inter-Society Color Council, The Colour Group (Great Britain), Canadian Society for Color, Color Science Association of Japan, Dutch Society for the Study of Color, The Swedish Colour Centre Foundation, Colour Society of Australia, Centre Français de la Couleur*, 26(5):340–350, 2001.
- [15] M Melgosa, E Hita, AJ Poza, David H Alman, and Roy S Berns. Suprathreshold color-difference ellipsoids for surface colors. *Color Research & Application: Endorsed by Inter-Society Color Council, The Colour Group (Great Britain), Canadian Society for Color, Color Science Association of Japan, Dutch Society for the Study of Color, The Swedish Colour Centre Foundation, Colour Society of Australia, Centre Français de la Couleur*, 22(3):148–155, 1997.
- [16] Alain Chardon, Isabelle Cretois, and Colette Hourseau. Skin colour typology and sun-tanning pathways. *International journal of cosmetic science*, 13(4):191–208, 1991.
- [17] S Del Bino, J Sok, E Bessac, and F Bernerd. Relationship between skin response to ultraviolet exposure and skin color type. *Pigment cell research*, 19(6):606–614, 2006.
- [18] Sonia A Lamel, Kristin M Haldeman, Haines Ely, Carrie L Kovarik, Hon Pak, and April W Armstrong. Application of mobile teledermatology for skin cancer screening. *Journal of the American Academy of Dermatology*, 67(4):576–581, 2012.
- [19] S Vañó-Galván, A Hidalgo, I Aguayo-Leiva, M Gil-Mosquera, L Ríos-Buceta, MN Plana, J Zamora, A Martorell-Calatayud, and P Jaén. Store-and-forward teledermatology: assessment of validity in a series of 2000 observations. *Actas Dermo-Sifiliográficas (English Edition)*, 102(4):277–283, 2011.
- [20] Cheng Chen, Qi Dou, Hao Chen, Jing Qin, and Pheng-Ann Heng. Synergistic image and feature adaptation: Towards cross-modality domain adaptation for medical image segmentation. In *Proceedings of the AAAI conference on artificial intelligence*, volume 33, pages 865–872, 2019.
- [21] David Tellez, Geert Litjens, Péter Bándi, Wouter Bulten, John-Melle Bokhorst, Francesco Ciompi, and Jeroen Van Der Laak. Quantifying the effects of data augmentation and stain color normalization in convolutional neural networks for computational pathology. *Medical image analysis*, 58:101544, 2019.

- [22] Hao Guan and Mingxia Liu. Domain adaptation for medical image analysis: a survey. *IEEE Transactions on Biomedical Engineering*, 69(3):1173–1185, 2021.
- [23] Norimichi Tsumura, Nobutoshi Ojima, Kayoko Sato, Mitsuhiro Shiraishi, Hideto Shimizu, Hirohide Nabeshima, Syuuichi Akazaki, Kimihiko Hori, and Yoichi Miyake. Image-based skin color and texture analysis/synthesis by extracting hemoglobin and melanin information in the skin. In *ACM SIGGRAPH 2003 Papers*, SIGGRAPH '03, page 770–779, New York, NY, USA, 2003. Association for Computing Machinery.
- [24] Georgios N Stamatias, Barbara Z Zmudzka, Nikiforos Kollias, and Janusz Z Beer. Non-invasive measurements of skin pigmentation in situ. *Pigment Cell Research*, 17(6):618–626, 2004.
- [25] Roxana Daneshjou, Kailas Vodrahalli, Roberto A. Novoa, Melissa Jenkins, Weixin Liang, Veronica Rotemberg, Justin Ko, Susan M. Swetter, Elizabeth E. Bailey, Olivier Gevaert, Pritam Mukherjee, Michelle Phung, Kiana Yekrang, Bradley Fong, Rachna Sahasrabudhe, Johan A. C. Allerup, Utako Okata-Karigane, James Zou, and Albert S. Chiou. Disparities in dermatology ai performance on a diverse, curated clinical image set. *Science Advances*, 8(32):eabq6147, 2022.
- [26] Matthew Groh, Caleb Harris, Luis Soenksen, Felix Lau, Rachel Han, Aerin Kim, Arash Koochek, and Omar Badri. Evaluating deep neural networks trained on clinical images in dermatology with the fitzpatrick 17k dataset. In *Proceedings of the IEEE/CVF conference on computer vision and pattern recognition*, pages 1820–1828, 2021.
- [27] Geunho Jung, Semin Kim, and Sangwook Yoo. Skin tone analysis through skin tone map generation with optical approach and deep learning. *Skin Research and Technology*, 30(10):e70088, 2024.
- [28] Valery Tuchin. Tissue optics light scattering methods and instruments for medial diagnosis. *SPIE*, 13, 01 2000.
- [29] Georgios N Stamatias and Nikiforos Kollias. Blood stasis contributions to the perception of skin pigmentation. *Journal of biomedical optics*, 9(2):315–322, 2004.
- [30] Igor V Meglinski and Stephen J Matcher. Quantitative assessment of skin layers absorption and skin reflectance spectra simulation in the visible and near-infrared spectral regions. *Physiological measurement*, 23(4):741, 2002.
- [31] Aravind Krishnaswamy and Gladimir VG Baranoski. A biophysically-based spectral model of light interaction with human skin. *Computer Graphics Forum*, 23(3):331–340, 2004.
- [32] Ayan Chakrabarti, Ying Xiong, Baochen Sun, Trevor Darrell, Daniel Scharstein, Todd Zickler, and Kate Saenko. Modeling radiometric uncertainty for vision with tone-mapped color images. *IEEE Transactions on Pattern Analysis and Machine Intelligence*, 36(11):2185–2198, 2014.

- [33] Marcus Wilkes, Caradee Y Wright, Johan L du Plessis, and Anthony Reeder. Fitzpatrick skin type, individual typology angle, and melanin index in an african population: steps toward universally applicable skin photosensitivity assessments. *JAMA dermatology*, 151(8):902–903, 2015.
- [34] A Fullerton, T Fischer, A Lahti, K-P Wilhelm, H Takiwaki, and J Serup. Guidelines for measurement skin colour and erythema a report from the standardization group of the european society of contact dermatitis. *Contact dermatitis*, 35(1):1–10, 1996.
- [35] Hirotosugu Takiwaki. Measurement of skin color: practical application and theoretical considerations. *The Journal of Medical Investigation*, 44(3–4):121–126, 1998.
- [36] Junichi Nakamura, editor. *Image Sensors and Signal Processing for Digital Still Cameras*. Optical Science and Engineering. CRC Press, Boca Raton, FL, 2005.
- [37] Eric R Fossum. Cmos image sensors: Electronic camera-on-a-chip. *IEEE Transactions on Electron Devices*, 44(10):1689–1698, 1997.
- [38] Adewole S. Adamson and Avery Smith. Machine learning and health care disparities in dermatology. *JAMA Dermatology*, 154(11):1247–1248, 11 2018.
- [39] Newton M. Kinyanjui, Timothy Odonga, Celia Cintas, Noel C. F. Codella, Rameswar Panda, Prasanna Sattigeri, and Kush R. Varshney. Fairness of classifiers across skin tones in dermatology. In *Medical Image Computing and Computer Assisted Intervention – MICCAI 2020*, pages 320–329, Cham, 2020. Springer International Publishing.
- [40] Olivia R Ware, Jessica E Dawson, Michi M Shinohara, and Susan C Taylor. Racial limitations of fitzpatrick skin type. *Cutis*, 105(2):77–80, 2020.
- [41] Korea Intelligence Information Society Agency. Korean skin condition measurement data. AI Hub, 2023.
- [42] Patrick E Shrout and Joseph L Fleiss. Intraclass correlations: uses in assessing rater reliability. *Psychological bulletin*, 86(2):420, 1979.
- [43] Terry K. Koo and Mae Y. Li. A guideline of selecting and reporting intraclass correlation coefficients for reliability research. *Journal of Chiropractic Medicine*, 15(2):155–163, 2016.
- [44] Leslie G. Portney and Mary P. Watkins. *Foundations of Clinical Research: Applications to Practice*. F.A. Davis Company, Philadelphia, 3rd edition, 2015.
- [45] J. Martin Bland and DouglasG. Altman. Statistical methods for assessing agreement between two methods of clinical measurement. *The Lancet*, 327(8476):307–310, 1986. Originally published as Volume 1, Issue 8476.
- [46] Jacob Cohen. *Statistical Power Analysis for the Behavioral Sciences*. Lawrence Erlbaum Associates, Hillsdale, NJ, 2nd edition, 1988.

- [47] Yao Pan, Xue Ma, Jinfeng Zhao, Shiyu Yan, Qi Liu, and Hua Zhao. The interaction of age and anatomical region influenced skin biophysical characteristics of chinese women. *Clinical, Cosmetic and Investigational Dermatology*, 13:911–926, 2020.
- [48] Mengmeng Wang, Kaida Xiao, Ming Ronnier Luo, Michael Pointer, Vien Cheung, and Sophie Wuerger. An investigation into the variability of skin colour measurements. *Color Research & Application*, 43(4):458–470, 2018.
- [49] MQ Man, SJ Xin, SP Song, SY Cho, XJ Zhang, CX Tu, KR Feingold, and PM Elias. Variation of skin surface ph, sebum content and stratum corneum hydration with age and gender in a large chinese population. *Skin pharmacology and physiology*, 22(4):190–199, 2009.
- [50] Huafeng Ding, Jun Q Lu, William A Wooden, Peter J Kragel, and Xin-Hua Hu. Refractive indices of human skin tissues at eight wavelengths and estimated dispersion relations between 300 and 1600 nm. *Physics in Medicine & Biology*, 51(6):1479–1489, 2006.
- [51] Karan Chopra, Daniel Calva, Michael Sosin, Kashyap Komarraju Tadisina, Abhishake Banda, Carla De La Cruz, Muhammad R. Chaudhry, Teklu Legesse, Cinithia B. Drachenberg, Paul N. Manson, and Michael R. Christy. A comprehensive examination of topographic thickness of skin in the human face. *Aesthetic Surgery Journal*, 35(8):1007–1013, 10 2015.
- [52] Boaz Arad and Ohad Ben-Shahar. Sparse recovery of hyperspectral signal from natural rgb images. In *Computer Vision – ECCV 2016*, pages 19–34, Cham, 2016. Springer International Publishing.
- [53] Zhan Shi, Chang Chen, Zhiwei Xiong, Dong Liu, and Feng Wu. Hscnn+: Advanced cnn-based hyperspectral recovery from rgb images. In *Proceedings of the IEEE Conference on Computer Vision and Pattern Recognition Workshops*, pages 939–947, 2018.
- [54] M. Raissi, P. Perdikaris, and G.E. Karniadakis. Physics-informed neural networks: A deep learning framework for solving forward and inverse problems involving nonlinear partial differential equations. *Journal of Computational Physics*, 378:686–707, 2019.
- [55] Ellis Monk. The monk skin tone scale, 2023.